Optimised Hydrogen Production by Aqueous Phase Reforming of Glycerol on Pt/Al_2O_3

Nachal D. Subramanian[a,b], June Callison[a,b], C. Richard A. Catlow[a,b], Peter P. Wells[a,b,*] and Nikolaos Dimitratos[a,c,*]

[a] UK Catalysis Hub, Research Complex at Harwell, Rutherford Appleton Laboratory, Harwell Oxon, Didcot, OX11 0FA, United Kingdom.
[b] Department of Chemistry, University College London, 20 Gordon Street, London WC1H 0AJ, United Kingdom.
[c] Cardiff Catalysis Institute, School of Chemistry, Cardiff University, Cardiff, CF10 3AT, United Kingdom.
*DimitratosN@cardiff.ac.uk; Peter.wells@rc-harwell.ac.uk

Abstract

Aqueous phase reforming of glycerol was studied over a series of γ-Al_2O_3 supported metal nanoparticle catalysts for hydrogen production in a batch reactor. Of the metals studied, Pt/Al_2O_3 was found to be the most active catalyst under the conditions tested. A further systematic study on the impact of reaction parameters, including stirring speed, pressure, temperature, and substrate/metal molar ratio, was conducted and the optimum conditions for hydrogen production (and kinetic regime) were determined as 240 °C, 42 bar, 1000 rpm, and substrate/metal molar ratio $\geq$ 4100 for a 10 wt% glycerol feed. The glycerol conversion and hydrogen yield achieved at these conditions were 18% and 17%, respectively, with negligible CO and CH_4 formation. Analysis of the spent catalyst using FTIR provides an indication that the reaction pathway includes glycerol dehydrogenation and dehydration steps in the liquid phase in addition to typical reforming and water gas shift reactions in the gas phase.

Keywords: Hydrogen, Aqueous phase reforming, Glycerol, Batch reactor

1. Introduction

The focus on mitigating global climate change and replacing petroleum based energy sources is growing rapidly which has boosted the research interest towards alternative and renewable energy strategies. Hydrogen production is one of the most important alternative energy technologies for meeting future global energy needs. It is environmentally clean and efficient, compared to conventional petroleum-based fuels [1-9]. Several biomass-derived oxygenated compounds such as methanol, sorbitol, glycerol, ethylene glycol, and ethanol have been studied in aqueous phase reforming (APR) processes to produce hydrogen [2, 4, 10]. Of

these, glycerol is of particular interest because of its ample availability (~10 wt%) as a by-product in biodiesel production from transesterification of vegetable oils or animal fats [1, 11-13]. With increasing biodiesel production, the crude glycerol is also consequently produced in substantial amounts and one of the promising ways to utilise this crude glycerol is to produce hydrogen and other value-added products by reforming processes [14-17].

APR of glycerol occurs according to the following stoichiometric reaction [1-4, 6, 11-13, 18, 19]:

$C_3H_8O_3 + 3H_2O \rightarrow 7H_2 + 3CO_2$ (1)

This can be broken down into glycerol decomposition (2) and the water gas shift reaction (3).

$C_3H_8O_3 \rightarrow 4H_2 + 3CO$ (2)

$CO + H_2O \rightarrow CO_2 + H_2$ (3)

The further reaction of CO and/or CO_2 with H_2 results in methanation or Fischer–Tropsch reactions, and other side reactions include methane dry reforming and/or decomposition, carbon monoxide disproportionation (Boudouard reaction), and carbon gasification. Thermodynamically, the APR process is favourable at significantly lower temperatures (~227 °C) and pressures high enough to keep water in the liquid phase, where the WGS reaction is facilitated. This makes it possible to generate hydrogen with low amounts of CO in the product stream [4, 9, 20]. In addition, the use of higher pressures in this process facilitates the effective purification of H_2-rich effluent by adsorption or membrane technology [4, 21]. Also, the APR process offers a greater possibility for directly using crude glycerol as the feedstock [15, 22].

The different reaction pathways that lead to various liquid and gaseous by-products during glycerol APR have been reported earlier and the main catalytic route for the production of H_2 involves the cleavage of C–C bonds as well as C–H and/or O–H bonds to form adsorbed

species on the catalyst surface [6, 12, 23, 24]. The catalyst must promote the WGS reaction for the removal of adsorbed CO species, but must not favour C–O bond cleavage and hydrogenation of adsorbed CO or CO_2, that lead to undesired by-products [1, 2, 23]. Dumesic and co-workers were the first to develop APR of various biomass-derived compounds. They reported that Group VIII metals, particularly Pt, Pd and Ni, were the most effective catalysts, with Pt being the best monometallic catalyst of all, in terms of activity and selectivity for APR [4, 25, 26]. Davda *et al.* found the reaction rates decreased in the order of Pt~Ni > Ru > Rh~Pd > Ir at temperatures from 210 to 225 °C [27]. Several supports have also been reported to influence the activity and selectivity of monometallic catalysts [23-36] and among the different supports investigated, Pt supported on γ-Al_2O_3 showed the highest hydrogen selectivity (>90%) [37].

Earlier studies have focussed mainly on the choice of catalysts for APR of glycerol, but not many systematic studies reported aimed at optimizing the reaction conditions for Pt/Al_2O_3 in a batch reactor. Ozgur *et al.* conducted a study of the effect of process variables on 1 wt% Pt/Al_2O_3 catalyst, however only the effect of temperature was investigated in a batch reactor [9]. Although this study provides insights on three important process variables, it does not provide the optimum conditions for a batch system. They also observed CO as a product in all their batch experiments (~5-8 mol%). In their case, the system pressure could not be maintained above the vapour pressure of water at all temperatures, and water was not kept in the liquid phase, which is essential for APR. Recently, Seretis *et al.*[38] studied the effect of reaction temperature, catalyst weight, and feed concentration over 5 wt% Pt/Al_2O_3 catalyst in a batch reactor, but the study did not include the effect of stirring speed, which is an essential parameter to ensure the reaction is not diffusion limited.

The focus of the present study is to address these important factors and to find the appropriate reaction conditions which favours the APR of glycerol for H_2 production with

negligible CO formation in a batch reactor. We present systematic studies of γ-Al_2O_3 supported metal catalysts supplied by Johnson Matthey UK and investigate the impact of reaction parameters in a batch reactor (stirring speed, pressure, temperature, and substrate/metal molar ratio) on the most promising Pt/Al_2O_3 catalyst. Our results also give insight into the reaction pathway.

2. Experimental

2.1. Catalyst Synthesis and Characterization

The catalysts studied for this work were prepared by Johnson Matthey UK, using their proprietary routes. Four research grade catalysts, namely, Pt/Al_2O_3, Pd/Al_2O_3, Au/Al_2O_3, and Rh/Al_2O_3 (all 2 wt% metal loading with γ-Al_2O_3 used as the support) were synthesized using incipient wetness impregnation method followed by calcination in air at 500 °C for 2 hours. No further activation treatments were carried out prior to reaction.

The catalysts were characterized by BET, Microwave plasma - atomic emission spectrometry (MP-AES), Energy dispersive X-ray spectroscopy (EDS), X-ray diffraction (XRD), transmission electron microscopy (TEM), and Fourier transform infrared spectroscopy (FTIR).

The surface area of the calcined catalysts was measured using the BET method. The samples were first degassed at 140 °C under vacuum using a FloVac Degasser. Analysis was then carried out on a Quadrasorb EVO instrument supplied by Quantachrome. The elemental analysis by MP-AES was performed using an Agilent 4100 Microwave Plasma-Atomic Emission Spectrometer. Solid samples were first digested in Aqua Regia using an Anton Paar Multiwave 3000 and then diluted in deionised water to form a 0.1 wt% solution. Standards were made up using 10% aqua regia and used to calibrate the instrument before the samples were run.

EDS analysis was performed on a JSM-6610LV scanning electron microscope (JEOL) fitted with Oxford Instruments Xmax 80mm EDS detector running Aztec analysis software. The powder samples were dispersed on conductive carbon tabs placed on aluminium stubs. XRD patterns were recorded on a Rigaku Miniflex 600 benchtop powder X-ray diffractometer equipped with a 6-position autosampler and Cu Kα radiation source. The 2θ angles were scanned from 5 to 80˚ at a rate of 5 ˚/min.

TEM experiments were carried out on a JEM-2100Plus electron microscope with a 200 kV accelerating voltage. Samples for TEM were prepared by dispersing the supported catalysts in methanol and then dropping the solution on 300 mesh carbon-coated copper grids. FTIR spectra were obtained using a Thermo Nicolet iS10 spectrometer with a DTGS detector. The sample was placed on the surface of a diamond crystal attenuated total reflectance (ATR) cell and spectra were collected at 2 cm^{-1} resolution and 32 scans.

2.2. Catalytic tests

Glycerol reforming APR was carried out in a 50 ml autoclave batch reactor (Parr Series 4590 Bench Top Micro Reactor equipped with magnetic drive stirrer and a Parr 4848B Reactor Controller system). The catalyst was mixed with 20 ml of 10 wt% aqueous glycerol solution. The reactor was sealed and the air inside was purged with argon few times before starting the reaction. The tests were performed at various stirring speeds (300 – 1500 rpm), pressures (28 – 49 bar), temperatures (225 – 265 °C), and substrate/metal molar ratios (3079 – 8210) to identify the optimum set of reaction conditions that leads to the best possible hydrogen yield and glycerol conversion.

Gas products were collected in a gas sampling bag after 2 hours of reaction and analyzed using a Shimadzu gas chromatograph system (GC-2014 with TCD and FID), equipped with Hayesep N and Mol Sieve 5A packed columns. In the liquid phase, the concentration of unreacted glycerol was analyzed by a Shimadzu Prominence HPLC installed

with a MetaCarb 67H column and RID-10A refractive index detector. Conversion was calculated based on the moles of glycerol consumed. The experiments could be reproduced with a relative error of 5%. Potential metal leaching into the reaction mixture was also analyzed using MP-AES analysis. For this, concentrated HCl was added to the spent reaction solution after filtering to produce a 10% HCl solution. Calibration standards were also made in 10% HCl. The minimum detection limit of the MP-AES instrument using this method was 100 ppb.

The catalyst reusability was tested using the following procedure. A reaction was carried out in the batch reactor as described above and the conversion was determined. An equivalent amount of feed solution (10 wt% aqueous glycerol), corresponding to the calculated conversion, was added to the same reactor and reaction started again. This procedure was followed for five consecutive cycles.

The glycerol conversion, H_2 yield and gas-phase product distribution (mol%) were calculated according to the following definitions:

$$\text{Glycerol conversion (\%)} = \frac{C0 - Ct}{C0} . 100$$

$$H_2 \text{ yield (\%)} = \frac{H_2 \text{ in product gas stream}}{\text{Theoretical } H_2 \text{ from complete reforming}} . 100$$

$$\text{Gas-phase product distribution (mol\%)} = \frac{\text{Moles of gas product i produced}}{\text{Total moles of gas products } (H_2, CO, CO_2, CH_4)} . 100$$

3. Results and Discussion

3.1. Materials Characterization

BET and elemental analysis results are provided in the Supporting Information (Table S1). Fig. 1 shows the XRD patterns for all catalysts and indicates the presence of characteristic peaks of γ-Al_2O_3 phase at 2θ = 20°, 33°, 37.5°, 39.8°, 46°, 61°, and 67°, in agreement with the literature [5, 39-41]. These peaks correspond to the (111), (220), (311), (222), (400), (511) and (440) reflections of γ-Al_2O_3 respectively [40, 41]. For Au/Al_2O_3, in addition to the typical peaks of the γ-Al_2O_3 phase, some additional peaks attributable to gold in the metallic state (2θ =

38.5°, 44.9° and 65°), were also observed [42]. The average gold crystallite size was estimated to be 7.4 nm (calculated using Scherrer equation for the Au(111) diffraction peak at 2θ = 38.5°). In the case of Pt, Pd, and Rh catalysts, the lack of clear reflections attributable to metallic phases indicates that the size domains are too small to be detected by conventional XRD. It is also difficult to carry out any structure identification of the metal phase due to the overlapping of their reflections with those of γ-alumina.

TEM was performed on all catalysts to determine the average particle (Fig. 2). From TEM, an average particle size of 1.6, 2.4, 4, and 7 nm was determined for Pt/Al_2O_3, Pd/Al_2O_3, Rh/Al_2O_3, and Au/Al_2O_3 catalysts, respectively. In the case of Au/Al_2O_3, the value of Au particle size obtained from TEM (7 nm) is close to the crystallite size value obtained from XRD data (7.4 nm).

FTIR analysis was performed on the catalysts to identify any adsorbed species that is present on the catalyst surface (See Supporting information, Fig. S1). The absence of any major IR bands other than weak vibrations due to adsorbed water suggested clean catalyst surfaces with no impurities prior to catalytic reaction.

3.2. Catalytic tests

This section compares the activities of all the catalysts and identifies the best catalyst on which further systematic studies were focused on. Fig. 3 summarises the glycerol conversion and H_2 yields for all the catalysts at 270 °C, P_{Ar} = 55 bar, 500 rpm, 3 wt% glycerol solution, and 60 mg catalyst (substrate/metal = 1232 mol/mol) after 4 h reaction time. Table 1 lists the H_2 TOFs, rates of production and other activity results. The products detected in the gas phase were only H_2, CH_4, and CO_2 (CO was negligible and below GC detection limits, which was 0.5% CO). Since the system pressure for the APR reaction was much higher than vapor pressure of water at all conditions tested in our study, the complete conversion of CO through water gas shift reaction could be achieved as reported elsewhere [9, 24].

From the results, it is clearly evident that Pt/Al_2O_3 showed the highest activity among all catalysts at similar reaction conditions. At 270 °C, Pt/Al_2O_3 showed almost complete conversion with the highest H_2 yield (35%). The other catalysts showed conversions below 20% and hydrogen yields less than 4%. The rates of H_2 production were also much lower compared to Pt/Al_2O_3 (Table 1). We should note that such high temperatures would lead to significant methane formation as well. Of all the catalysts, Pd/Al_2O_3 showed the highest methane formation of 7.3 mol%. Among the four catalysts tested, Pt/Al_2O_3 is the most active catalyst for glycerol reforming. This catalyst was chosen to conduct further systematic studies in order to optimize the reaction conditions. The remaining study is thus focused on exploring the effects of various reaction variables (stirring speed, pressure, temperature, and substrate/metal molar ratio) and to identify the kinetic regime for the most active Pt/Al_2O_3 catalyst.

4. Optimisation of glycerol reforming conditions over the most active Pt/Al_2O_3 catalyst

4.1. Effect of stirring speed

The effect of stirring speed on catalytic performance was studied in order to exclude the presence of mass transfer effects which might limit the rate of reaction. Fig. 4 shows the effect of stirring speed on glycerol conversion, H_2 yield, and gas-phase product distribution for the Pt/Al_2O_3 catalyst at 240 °C, 42 bar, 10 wt% glycerol solution, and 60 mg catalyst (substrate/metal = 4105 mol/mol) after 2 h of reaction.

The glycerol conversion increases steadily up to 1000 rpm (Fig. 4a) after which it remains almost constant, making 1000 rpm the optimum stirring speed to avoid any diffusion limitations. This observation suggests that at lower stirring rates, the transfer of glycerol from the bulk to the catalyst surface is rate-limiting. The molar ratio of H_2 to CO_2 for these tests was higher than the theoretical ratio of 2.33 (between 2.7 and 3.0), which indicated the occurrence of other hydrogen producing reactions such as WGS or dehydrogenation besides the main APR

reaction [2, 43]. The major products in the gas phase are H_2 and CO_2, with much less CH_4. There is no significant change in product distribution with change in stirring speed (Fig. 4b) and the most remarkable feature to be noted is the methane suppression at all conditions tested in this study (less than 1 mol% methane at all stirring speeds). With increase in stirring speed, as we approach the surface reaction limited kinetic regime, the initially formed hydrogen participates in further reactions, thereby decreasing its yield.

4.2. Effect of temperature

The reaction temperature serves as one of the most important parameters which has a significant effect on the rate and selectivity of kinetically controlled reactions. It is known that methane formation is thermodynamically favorable at all temperatures and so methanation must be kinetically limited in order to increase hydrogen yield and selectivity.

The influence of reaction temperature on glycerol conversion and H_2 yield for the Pt/Al_2O_3 catalyst is presented in Fig. 5. Table 2 lists the corresponding product selectivities, rates of H_2 production and TOFs of H_2 and glycerol.

The increase of reaction temperature from 225 to 265 °C results in an increase of glycerol conversion from 10% to 47%. As a result, the rate of H_2 production is more than 20 times higher at 265 °C compared to 225 °C. Hydrogen distribution (mol%) decreases while that of CO_2 increases with increase in reaction temperature due to the higher conversions achieved at higher temperatures (Table 2), as reported by Seretis *et al.*[38] Although the conversions and H_2 yields are very high at increased temperatures (47% conversion and 52% H_2 yield at 265 °C), the formation of undesired methane also increased remarkably at the expense of hydrogen. This behavior is expected from a thermodynamic point of view, because thermodynamically, glycerol reforming is a highly endothermic reaction, and hence higher temperatures lead to higher hydrogen yields, but also methanation. Cortright *et al.* studied the APR of sugars and alcohols for H_2 production using a Pt-based catalyst and found that high

operating temperatures resulted in low H_2 selectivity, high alkane selectivity, but high biomass conversions [25]. Similar trends were reported by Ozgur *et al.* on 1 wt-% Pt/Al_2O_3 catalyst [9]. The results from this study clearly demonstrate that 240 °C is the optimum temperature.

4.3. Effect of pressure

Fig. 6 shows the effect of total pressure on glycerol conversion, product selectivities, and H_2 yield for the Pt/Al_2O_3 catalyst at 240 °C, 1000 rpm, 10 wt% glycerol solution, and 60 mg catalyst (substrate/metal = 4105 mol/mol) after 2 h of reaction. With increase in pressure, the conversion goes through a maximum of 17.9% at 42 bar.

Lower pressure leads to a higher H_2 yield of 46.7%, but the conversion is only 12.2%. At this pressure, 28 bar, which is the autogenous pressure at 240 °C, the H_2/CO_2 molar ratio was much higher (3.37) as compared to that at all other conditions tested in this study (range from 2.2 to 3.0). In most of our experiments, the H_2/CO_2 ratio was found to be typically higher than the stoichiometry of the reforming reaction (H_2/CO_2 = 2.33), which suggests that more hydrogen was being produced by a secondary reaction like WGS or dehydrogenation. This result also shows that the hydrogen formed via the reforming or WGS reaction is not being used for the hydrogenation of any unsaturated intermediates, as was the case reported by Wawrzetz *et al.*[43]. They observed a H_2/CO_2 ratio of ~1.9, which they attributed the difference to a fraction of hydrogen being used for the hydrogenation of unsaturated intermediates. In our case, the results suggest that the hydrogen formed was not being used for any further hydrogenation reactions. When compared to studies at similar conditions, the TOF values obtained in our study are significantly higher. Wawrzetz *et al.*[43] reported a H_2 TOF of ~3 $mol.mol_{Pt}^{-1}.min^{-1}$ and CO_2 TOF of ~0.9 $mol.mol_{Pt}^{-1}.min^{-1}$ at 225 °C and 29 bar on a 3 wt% Pt/Al_2O_3 catalyst and 10 wt% glycerol solution. At 240 °C and 28 bar on a 2 wt% Pt/Al_2O_3 catalyst and 10 wt% glycerol solution, our TOF values are H_2 = 13.1 and CO_2 = 3.9 $mol.mol_{Pt}^{-1}.min^{-1}$.

4.4. Effect of substrate/metal molar ratio

Table 3 shows the activity results at different substrate/metal molar ratios (SMMR), which was performed to identify the regime in which the reaction is kinetically limited. Initially, the experiments were carried out at substrate/metal molar ratios of 6158, 4105 and 3079 mol/mol, corresponding to 40, 60 and 80 mg of catalyst, respectively. From the results, it was observed that by decreasing the SMMR from 6158 to 4105, the conversion increased more than two-fold, from 7.9 to 17.9%. This increase in conversion can be attributed to an increase in the number of active sites due to the increase in the mass of catalyst used. But a further decrease of the SMMR to 3079 (increase of the catalyst mass to 80 mg) resulted in a slight decrease in conversion to 16.9%, suggesting that a higher number of active sites than required were now available. The continuous increase in conversion with decrease in SMMR up to 4105 indicates that the reaction is kinetic controlled when the ratio is $\geq$ 4100. The reaction becomes diffusion limited at lower SMMRs. To confirm this proposal and to identify the optimum range of SMMR, two more tests were carried out (using 30 mg and 50 mg catalyst corresponding to SMMRs of 8210 and 4926 respectively). Fig. 7 shows the effect of different substrate/metal molar ratios on glycerol conversion. The conversion increases almost linearly with decrease in SMMR up to 4105 mol/mol. This confirms the above hypothesis that the reaction is in the kinetic regime when the substrate/metal molar ratio is 4100 or higher.

From all the above series of experiments, the optimum set of reaction conditions to achieve the best possible hydrogen yield and glycerol conversion were identified as 240 °C, 42 bar, 1000 rpm, and SMMR $\geq$ 4100 for a 10 wt% glycerol feed. At these best set of conditions, the other γ-Al_2O_3 supported JM catalysts were tested again for comparison and the results are presented in the Supporting Information (Fig. S2). Pt/Al_2O_3 was found to be the most active catalyst at all conditions.

5. Metal leaching and catalyst reusability

The spent reaction mixtures were analyzed for any potential metal leaching into the solutions using MP-AES. The result showed that the Pt concentration in the reaction solution was less than the detection limit (i.e., 100 ppb), which corresponds to less than 0.2% of the starting Pt used. The same result was obtained with reactions carried out at all conditions, indicating that there is no discernable leaching of Pt.

As deactivation is a common phenomenon in liquid phase reactions, the Pt/Al_2O_3 catalyst was subjected to five reaction cycles without any pre-treatment between the tests, as described in the experimental section. The performance upon re-use is illustrated in Fig. 8 (Reaction conditions: 46 bar, 240 °C, 1000 rpm, 60 mg catalyst, and 10 wt% glycerol solution after 2 h reaction time). The results show that there is a slight increase in conversion at the end of the second cycle, after which there is a gradual decrease with further use. The drop in activity over five consecutive cycles is within ~35% of the initial conversion. Conversely, conversion towards gas products, and therefore hydrogen yield, decreases significantly, accompanied by a gradual increase in the liquid phase products.

Many catalyst reusability studies in literature also reported a severe drop in catalytic activity, which they attributed to catalytic dissolution / leaching [44, 45]. In our study, MP-AES tests of the spent liquid after reaction confirmed that there was no leaching of Pt into the solution. The other causes for the decrease in activity could be deactivation of the catalyst over time due to agglomeration or metal sintering.

The spent catalyst was analyzed using TEM after reaction. Fig. 9 shows the TEM images and corresponding histogram of the spent Pt/Al_2O_3 catalyst after a 2h reaction at 240 °C, 42 bar, 1000 rpm, and 10 wt% glycerol solution (at the end of first reaction cycle). The particle size distribution of used catalyst is similar to that of fresh catalyst (Section 3.1), with a mean particle size of 2 nm. After five reaction cycles, the mean particle size of the spent

catalyst obtained from TEM was ~2.1 nm. This result suggests that there was no significant increase in size even after five consecutive experiments and the structural stability of the catalyst under the reaction conditions remained intact. Therefore, the decrease in catalytic activity with the re-use of catalyst cannot be correlated to increase in particle size or sintering. The decrease in conversion can thus be related to the loss of the catalyst during filtration for liquid analysis after each cycle. A similar observation has also been reported for Cu-based catalysts during recycling studies [46, 47], which they attributed the handling losses of the catalyst during the reaction as the essential factor leading to the decrease in glycerol conversion.

6. Insights into reaction pathways using FTIR

The spent catalysts were also analyzed using FTIR after reaction for obtaining insights into possible reaction pathways. The FTIR spectra of the spent catalyst after reaction together with that of fresh Pt/Al_2O_3 catalyst and pure glycerol are shown in Fig. 10. In the case of fresh catalyst, a weak band at 1640 cm^{-1}, accompanied by a broad band in the range 3000-3700 cm^{-1} can be attributed to the OH bending and stretching vibrations of adsorbed water on the catalyst surface [43, 48]. In the case of pure glycerol and spent catalyst samples, the bands at ~1670 and 3000-3600 cm^{-1} can be assigned to the OH bending and stretching vibrations, that is typical for alcohols [49]. The intense band at ~1040 cm^{-1}, which is present in both glycerol and spent catalyst samples, can be assigned to the C-O stretching vibration that is characteristic of glycerol [50]. The doublet band in the 2900 cm^{-1} region (bands at 2877 and 2940 cm^{-1}) is also present in both glycerol and spent catalyst samples and can be attributed to the asymmetric and symmetric C-H stretching vibrations [48, 51]. In addition to these common features, the spent catalyst showed one unique feature of interest, a strong band at 1729 cm^{-1} accompanied by a broad band in the 2400-2700 cm^{-1} region. This can be assigned to the C=O and O-H valent vibrations of carbonyl groups, such as those found in carboxylic acids, ketones and aldehydes

[43, 49]. These bands are in good agreement with those observed for hydroxyacetone (1717 cm^{-1}), glyceraldehyde (1745 cm^{-1}) and pyruvaldehyde (1728 cm^{-1}) as shown by Wawrzetz *et al.* using FTIR spectroscopic experiments [43]. Hydroxyacetone is formed by the dehydration of glycerol which on further hydrogenation leads to propylene glycol formation. Glyceraldehyde is formed by the dehydrogenation of glycerol, which on further dehydration forms pyruvaldehyde, and subsequently gets converted to lactic acid.

The presence of keto and aldehyde carbonyl surface intermediates indicates that dehydration and dehydrogenation of glycerol are the dominating pathways in the liquid phase in addition to typical reforming and water gas shift reactions in the gas phase. The catalytic results in our study also showed a H_2/CO_2 molar ratio higher than the theoretical reforming ratio, which supports the occurrence of other hydrogen producing reactions such as dehydrogenation.

An analysis of the liquid products on the HPLC showed the presence of several unknown peaks. The results are presented in the Supporting Information (Fig. S3). On comparison with HPLC data of possible glycerol APR products (such as ethanol, acetaldehyde, ethylene glycol, propylene glycol, hydroxyacetone, glyceraldehyde and lactic acid), the unknown peaks matched with those of hydroxyacetone, ethylene glycol, propylene glycol, glyceraldehyde and lactic acid, indicating they were the most probable liquid products. Thus, combining the catalytic results with FTIR findings, we can conclude that ketones and aldehydes were the primary surface intermediates and that the APR reaction proceeded via dehydrogenation and dehydration of glycerol on a parallel route to reforming and WGS reactions. To gain a more precise understanding of adsorbed species on to the catalyst surface and to derive a complete reaction mechanism, more detailed *in situ* FTIR studies need to be performed.

7. Conclusions

A series of γ-Al_2O_3 supported metal nanoparticle catalysts were tested for glycerol APR to hydrogen in a batch reactor and the Pt/Al_2O_3 catalyst was found to be the most active and selective catalyst under the conditions tested. The present investigation indicates that the catalytic performance of the Pt catalyst is strongly influenced by stirring speed, reaction temperature, pressure, and substrate/metal molar ratio. It was observed that the formation of undesired products, especially methane, can be suppressed under certain reaction conditions. For the most active Pt/Al_2O_3 catalyst, these optimum conditions were found to be 240 °C, 42 bar, 1000 rpm, and SMMR ≥ 4100 for reactions carried out using 10 wt% glycerol feed. Analysis of spent catalyst using FTIR showed the presence of adsorbed carbonyl surface intermediates, which when coupled with the catalytic results, gave an indication that the reaction proceeded via dehydrogenation and dehydration of glycerol in addition to typical reforming and water gas shift reactions.

The product distribution with time-on-stream has to be studied in detail to understand the stability of the catalysts over longer reaction periods. Continuous reaction studies in a flow reactor will be our near future work as it permits detailed kinetic studies, rapid optimisation of reaction conditions, and assessment of the reusability of the catalyst in a single experiment as opposed to multiple experiments in conventional batch reactor screening.

Acknowledgements

The UK Catalysis Hub is kindly thanked for resources and support provided via our membership of the UK Catalysis Hub Consortium and funded by EPSRC (portfolio grants EP/K014706/1, EP/K014668/1, EP/K014854/1 and EP/K014714/1). We would like to thank the EPSRC for supporting the activities of the UK Catalysis Hub at (Catalytic Science in the Harwell Research Centre EP/ I019693/1). The staff at the RCaH are thanked for their continued support. The authors thank Johnson Matthey and Paul Collier for supplying the catalysts used

in this work. Kristina Penman is thanked for performing the MP-AES measurements. We would like to thank Gavin Stenning for help on the MiniFlex instrument in the Materials Characterization Laboratory at the ISIS Neutron and Muon Source.

References

[1] Manfro RL, da Costa AF, Ribeiro NFP, Souza MMVM. Hydrogen production by aqueous-phase reforming of glycerol over nickel catalysts supported on CeO_2. Fuel Processing Technology. 2011; 92: 330-5.

[2] Tuza PV, Manfro RL, Ribeiro NFP, Souza MMVM. Production of renewable hydrogen by aqueous-phase reforming of glycerol over Ni-Cu catalysts derived from hydrotalcite precursors. Renewable Energy. 2013; 50: 408-14.

[3] Wen G, Xu Y, Ma H, Xu Z, Tian Z. Production of hydrogen by aqueous-phase reforming of glycerol. International Journal of Hydrogen Energy. 2008; 33: 6657-66.

[4] Davda RR, Shabaker JW, Huber GW, Cortright RD, Dumesic JA. A review of catalytic issues and process conditions for renewable hydrogen and alkanes by aqueous-phase reforming of oxygenated hydrocarbons over supported metal catalysts. Appl Catal B. 2005; 56: 171-86.

[5] Menezes AO, Rodrigues MT, Zimmaro A, Borges LEP, Fraga MA. Production of renewable hydrogen from aqueous-phase reforming of glycerol over Pt catalysts supported on different oxides. Renewable Energy. 2011; 36: 595-9.

[6] Calles JA, Carrero A, Vizcaino AJ, Garcia-Moreno L. Hydrogen production by glycerol steam reforming over SBA-15-supported nickel catalysts: Effect of alkaline earth promoters on activity and stability. Catalysis Today. 2014; 227: 198-206.

[7] Manfro RL, Souza MMVM. Production of Renewable Hydrogen by Glycerol Steam Reforming Using Ni-Cu-Mg-Al Mixed Oxides Obtained from Hydrotalcite-like Compounds. Catalysis Letters. 2014; 144: 867-77.

[8] Wen G, Xu Y, Wei Y, Pei R, Li K, Xu Z, et al. Hydrogen Production by Aqueous-Phase Reforming of Biomass over Supported Pt Catalysts. Chinese Journal of Catalysis. 2009; 30: 830-5.

[9] Ozgur DO, Uysal BZ. Hydrogen production by aqueous phase catalytic reforming of glycerine. Biomass & Bioenergy. 2011; 35: 822-6.

[10] Kim HD, Park HJ, Kim TW, Jeong KE, Chae HJ, Jeong SY, et al. Hydrogen production through the aqueous phase reforming of ethylene glycol over supported Pt-based bimetallic catalysts. International Journal of Hydrogen Energy. 2012; 37: 8310-7.

[11] Dou B, Song Y, Wang C, Chen H, Xu Y. Hydrogen production from catalytic steam reforming of biodiesel byproduct glycerol: Issues and challenges. Renewable & Sustainable Energy Reviews. 2014; 30: 950-60.

[12] Franchini CA, Aranzaez W, Duarte de Farias AM, Pecchi G, Fraga MA. Ce-substituted $LaNiO_3$ mixed oxides as catalyst precursors for glycerol steam reforming. Applied Catalysis B-Environmental. 2014; 147: 193-202.

[13] Shao S, Shi A-W, Liu C-L, Yang R-Z, Dong W-S. Hydrogen production from steam reforming of glycerol over Ni/CeZrO catalysts. Fuel Processing Technology. 2014; 125: 1-7.

[14] Adhikari S, Fernando SD, Haryanto A. Hydrogen production from glycerol: An update. Energy Conversion and Management. 2009; 50: 2600-4.

[15] Gupta M, Kumar N. Scope and opportunities of using glycerol as an energy source. Renewable & Sustainable Energy Reviews. 2012; 16: 4551-6.

[16] Stelmachowski M. UTILIZATION OF GLYCEROL, A BY-PRODUCT OF THE TRANSESTRIFICATION PROCESS OF VEGETABLE OILS: A REVIEW. Ecological Chemistry and Engineering S-Chemia I Inzynieria Ekologiczna S. 2011; 18: 9-30.

[17] Vaidya PD, Rodrigues AE. Glycerol Reforming for Hydrogen Production: A Review. Chemical Engineering & Technology. 2009; 32: 1463-9.

[18] Seung-hoon K, Jae-sun J, Eun-hyeok Y, Kwan-Young L, Ju MD. Hydrogen production by steam reforming of biomass-derived glycerol over Ni-based catalysts. Catalysis Today. 2014; 228: 145-51.

[19] Wei Y, Lei H, Liu Y, Wang L, Zhu L, Zhang X, et al. Renewable Hydrogen Produced from Different Renewable Feedstock by Aqueous-Phase Reforming Process. Journal of Sustainable Bioenergy Systems. 2014; 4: 113-27.

[20] Tokarev AV, Kirilin A, V., Murzina EV, Eranen K, Kustov LM, Murzin DY, et al. The role of bio-ethanol in aqueous phase reforming to sustainable hydrogen. International Journal of Hydrogen Energy. 2010; 35: 12642-9.

[21] Doukkali ME, Iriondo A, Cambra JF, Arias PL. Recent Improvement on H_2 Production by Liquid Phase Reforming of Glycerol: Catalytic Properties and Performance, and Deactivation Studies. Topics in Catalysis. 2014; 57: 1066-77.

[22] Lehnert K, Claus P. Influence of Pt particle size and support type on the aqueous-phase reforming of glycerol. Catalysis Communications. 2008; 9: 2543-6.

[23] Huber GW, Dumesic JA. An overview of aqueous-phase catalytic processes for production of hydrogen and alkanes in a biorefinery. Catalysis Today. 2006; 111: 119-32.

[24] Luo N, Fu X, Cao F, Xiao T, Edwards PP. Glycerol aqueous phase reforming for hydrogen generation over Pt catalyst - Effect of catalyst composition and reaction conditions. Fuel. 2008; 87: 3483-9.

[25] Cortright RD, Davda RR, Dumesic JA. Hydrogen from catalytic reforming of biomass-derived hydrocarbons in liquid water. Nature. 2002; 418: 964-7.

[26] Huber GW, Shabaker JW, Dumesic JA. Raney Ni-Sn catalyst for H-2 production from biomass-derived hydrocarbons. Science. 2003; 300: 2075-7.

[27] Davda RR, Shabaker JW, Huber GW, Cortright RD, Dumesic JA. Aqueous-phase reforming of ethylene glycol on silica-supported metal catalysts. Applied Catalysis B-Environmental. 2003; 43: 13-26.

[28] Adhikari S, Fernando SD, To SDF, Bricka RM, Steele PH, Haryanto A. Conversion of glycerol to hydrogen via a steam reforming process over nickel catalysts. Energy & Fuels. 2008; 22: 1220-6.

[29] Bowker M, Davies PR, Al-Mazroai LS. Photocatalytic Reforming of Glycerol over Gold and Palladium as an Alternative Fuel Source. Catalysis Letters. 2009; 128: 253-5.

[30] Dou B, Wang C, Song Y, Chen H, Xu Y. Activity of Ni-Cu-Al based catalyst for renewable hydrogen production from steam reforming of glycerol. Energy Conversion and Management. 2014; 78: 253-9.

[31] Sanchez EA, Comelli RA. Hydrogen by glycerol steam reforming on a nickel-alumina catalyst: Deactivation processes and regeneration. International Journal of Hydrogen Energy. 2012; 37: 14740-6.

[32] Sanchez EA, Comelli RA. Hydrogen production by glycerol steam-reforming over nickel and nickel-cobalt impregnated on alumina. International Journal of Hydrogen Energy. 2014; 39: 8650-5.

[33] Wei L, Li K, Ma Y. Thermodynamic Analysis of Glycerol Steam Reforming using Calcium Oxide and Iron Oxide for High-Purity Hydrogen Production. International Journal of Chemical Reactor Engineering. 2012; 10.

[34] Zhang B, Tang X, Li Y, Xu Y, Shen W. Hydrogen production from steam reforming of ethanol and glycerol over ceria-supported metal catalysts. International Journal of Hydrogen Energy. 2007; 32: 2367-73.

[35] Pompeo F, Santori G, Nichio NN. Hydrogen and/or syngas from steam reforming of glycerol. Study of platinum catalysts. International Journal of Hydrogen Energy. 2010; 35: 8912-20.

[36] Sad ME, Duarte HA, Vignatti C, Padro CL, Apesteguia CR. Steam reforming of glycerol: Hydrogen production optimization. International Journal of Hydrogen Energy. 2015; 40: 6097-106.

[37] Shabaker JW, Huber GW, Davda RR, Cortright RD, Dumesic JA. Aqueous-Phase Reforming of Ethylene Glycol Over Supported Platinum Catalysts. Catalysis Letters. 2003; 88 1-8.

[38] Seretis A, Tsiakaras P. Aqueous phase reforming (APR) of glycerol over platinum supported on Al_2O_3 catalyst. Renewable Energy. 2016; 85: 1116-26.

[39] Rahman MM, Church TL, Variava MF, Harris AT, Minett AI. Bimetallic Pt-Ni composites on ceria-doped alumina supports as catalysts in the aqueous-phase reforming of glycerol. Rsc Advances. 2014; 4: 18951-60.

[40] Rozita Y, Brydson R, Scott AJ. An investigation of commercial gamma-Al_2O_3 nanoparticles. Journal of Physics: Conference Series. 2010; 241: 1-4.

[41] Samain L, Jaworski A, Edén M, Ladd D, Seo D-K, Garcia-Garcia FJ, et al. Structural analysis of highly porous γ-Al_2O_3. Journal of Solid State Chemistry. 2014; 217: 1-8.

[42] Luciani S, Cavani F, Dal Santo V, Dimitratos N, Rossi M, Bianchi C. The mechanism of surface doping in vanadyl pyrophosphate, catalyst for n-butane oxidation to maleic anhydride: The role of Au promoter. Catalysis Today. 2011; 169: 200-6.

[43] Wawrzetz A, Peng B, Hrabar A, Jentys A, Lemonidou AA, Lercher JA. Towards understanding the bifunctional hydrodeoxygenation and aqueous phase reforming of glycerol. J Catal. 2010; 269: 411-20.

[44] Leng Y, Wang J, Zhu D, Shen L, Zhao P, Zhang M. Heteropolyanion-based ionic hybrid solid: A green bulk-type catalyst for hydroxylation of benzene with hydrogen peroxide. Chemical Engineering Journal. 2011; 173: 620-6.

[45] Mootabadi H, Salamatinia B, Bhatia S, Abdullah A. Ultrasonic-assisted biodiesel production process from palm oil using alkaline earth metal oxides as the heterogeneous catalysts. Fuel. 2010; 89: 1818-25.

[46] Montassier C, Dumas JM, Granger P, Barbier J. Deactivation of supported copper based catalysts during polyol conversion in aqueous phase. Applied Catalysis A: General. 1995; 121: 231-44.

[47] Pudi SM, Biswas P, Kumar S, Sarkar B. Selective Hydrogenolysis of Glycerol to 1,2-Propanediol Over Bimetallic Cu-Ni Catalysts Supported on γ-Al_2O_3. Journal of the Brazilian Chemical Society. 2015; 26: 1551-64.

[48] Vignatti C, Avila MS, Apesteguia CR, Garetto TF. Catalytic and DRIFTS study of the WGS reaction on Pt-based catalysts. International Journal of Hydrogen Energy. 2010; 35: 7302-12.

[49] Lugovskoy S, Nisnevitch M, Lugovskoy A, Zinigrad M. Mechanochemical synthesis of dispersed layer composites on the basis of talc and a series of biological active species. Clean Technologies and Environmental Policy. 2009; 11: 277-82.

[50] Gorinstein S, Kitov S, Deutsch J. Spectroscopic determination of glycerol, polyphenols, and nitrogenous compounds in beer and wine. MBAA Technical Quarterly. 1980; 17: 156-9.

[51] Boga DA, Liu F, Bruijnincx PCA, Weckhuysen BM. Aqueous-phase reforming of crude glycerol: effect of impurities on hydrogen production. Catalysis Science & Technology. 2016; 6: 134-43.

Table 1. Activity results at 270 °C, 55 bar, 500 rpm, 3 wt% glycerol solution, 60 mg catalyst after 4 h of reaction for Pd/Al_2O_3, Au/Al_2O_3, Rh/Al_2O_3 and Pt/Al_2O_3 catalysts

Catalyst	H_2/CO_2	Gas product distribution (mol%)			Rate of H_2 production ($mmol.g_M^{-1}.hr^{-1}$)	H_2 TOF ($mol.mol_M^{-1}.hr^{-1}$)
		H_2	CO_2	CH_4		
Pd/Al_2O_3	5.1	77.4	15.3	7.3	113.8	12.1
Au/Al_2O_3	4.8	82.8	17.2	0	30.6	6.04
Rh/Al_2O_3	4.0	73.2	18.2	1.3	278.9	28.7
Pt/Al_2O_3	3.4	74.8	22.3	2.9	3592.3	700.9

Table 2. Effect of temperature over the Pt/Al_2O_3 catalyst at P_{Ar} = 42 bar, 1000 rpm, 60 mg catalyst, and 10 wt% glycerol after 2 h.

Temperature (°C)	H_2/CO_2	Gas product distribution (mol%)			TOF ($mol.mol_{Pt}^{-1}.hr^{-1}$)[a]		Rate of H_2 production ($mmol.g_{Pt}^{-1}.hr^{-1}$)[a]
		H_2	CO_2	CH_4	H_2 produced	GL converted	
225	3.0	75.1	24.9	0	136.4	212.2	699.1
240	2.8	73.4	25.9	0.7	434.0	368.0	2224.6
250	2.2	66.6	30.7	2.7	543.6	517.9	2786.3
265	2.7	68.9	26.0	5.1	3018.0	957.0	15469.0

[a] The Pt wt% value obtained from MP-AES was used for the rate and TOF calculations.

Table 3. Effect of substrate/metal molar ratio over the Pt/Al_2O_3 catalyst at 240 °C, P_{Ar} = 42 bar, 1000 rpm, and 10 wt% glycerol solution after 2 h of reaction

Catalyst weight (mg) / SMMR	Glycerol conversion (%)	H_2 Yield (%)	H_2/CO_2
30 / 8210	4.96	7.01	2.99
40 / 6158	7.90	15.19	2.73
50 / 4926	13.93	13.01	2.53
60 / 4105	17.92	16.68	2.83
80 / 3079	16.93	21.23	2.83

Captions for Figures

Fig. 1. XRD patterns for the fresh catalysts (a) Pt/Al_2O_3 (b) Rh/Al_2O_3 (c) Pd/Al_2O_3 (d) Au/Al_2O_3.

Fig. 2. Representative TEM images of the fresh catalysts (a) Pt/Al_2O_3 (b) Pd/Al_2O_3 (c) Au/Al_2O_3 (d) Rh/Al_2O_3 and (e) corresponding particle size distribution for the Pt/Al_2O_3 catalyst.

Fig. 3. Glycerol conversion (●) and H_2 yield (■) for Pd/Al_2O_3, Au/Al_2O_3, Rh/Al_2O_3 and Pt/Al_2O_3 catalysts. Reaction conditions: 270 °C, P_{Ar} = 55 bar, 500 rpm, 3 wt% glycerol, 60 mg catalyst, substrate/metal = 1232 mol/mol, 4 h reaction time.

Fig. 4. Effect of stirring speed on (a) glycerol conversion [■] and H_2 yield [●] (b) H_2 [♦], CO_2 [▼], and CH_4 [▲] gas product distribution (mol%) for the Pt/Al_2O_3 catalyst. Reaction conditions: 240 °C, P_{Ar} = 42 bar, 60 mg catalyst, and 10 wt% glycerol solution after 2 h.

Fig. 5. Effect of temperature on glycerol conversion [■] and H_2 yield [●] for the Pt/Al_2O_3 catalyst Reaction conditions: P_{Ar} = 42 bar, 1000 rpm, 60 mg catalyst, and 10 wt% glycerol solution after 2 h.

Fig. 6. Effect of pressure on glycerol conversion [■], H_2 yield [●], and H_2 [▲] and CO_2 [Δ] gas product distribution (mol%) for the Pt/Al_2O_3 catalyst. Reaction conditions: 240 °C, 1000 rpm, 60 mg catalyst, and 10 wt% glycerol solution after 2 h.

Fig. 7. Effect of substrate/metal molar ratio on glycerol conversion for the Pt/Al_2O_3 catalyst. Reaction conditions: 240 °C, 42 bar, 1000 rpm, and 10 wt% glycerol solution after 2 h.

Fig. 8. Reusability tested up to five consecutive cycles - glycerol conversion [■], H_2 yield [●] and TOF of H_2 produced (▲, right side axis) for the Pt/Al_2O_3 catalyst. Reaction conditions: P_{Ar} = 46 bar, 240 °C, 1000 rpm, 60 mg catalyst, and 10 wt% glycerol solution after 2 h.

Fig. 9. Representative TEM images and histogram of the spent Pt/Al_2O_3 catalyst after 2h reaction at 240 °C, 42 bar, 1000 rpm, and 10 wt% glycerol solution.

Fig. 10. FTIR spectra of (a) fresh Pt/Al_2O_3 catalyst before reaction (b) pure glycerol and (c) spent catalyst after 2h reaction at 240 °C, 42 bar, 1000 rpm, and 10 wt% glycerol solution (Note: the spectra of fresh catalyst (a) has been zoomed in to see clearly).

Fig. 1

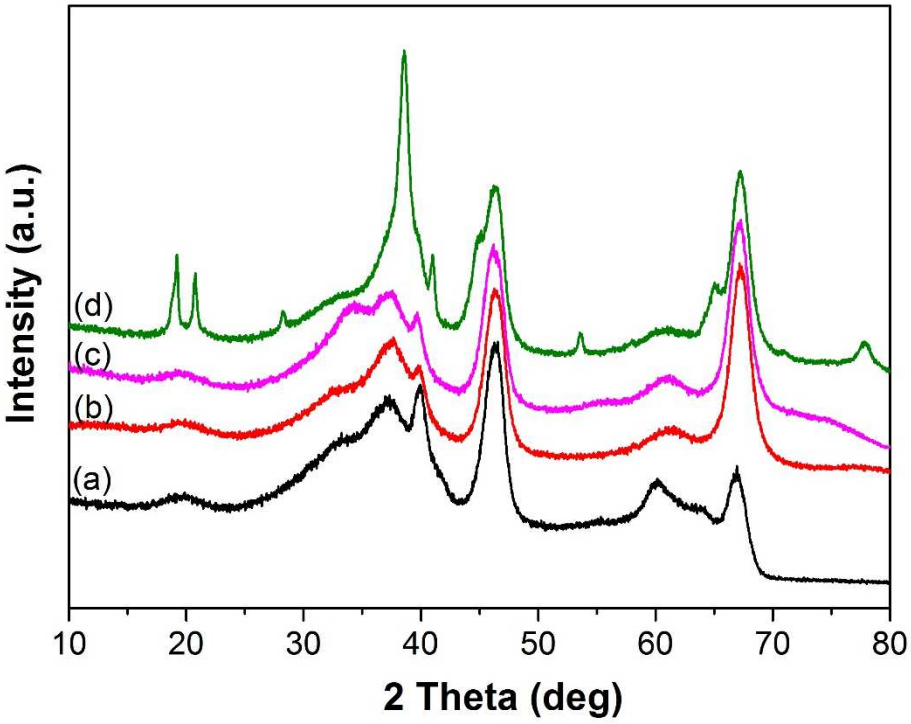

Fig. 2

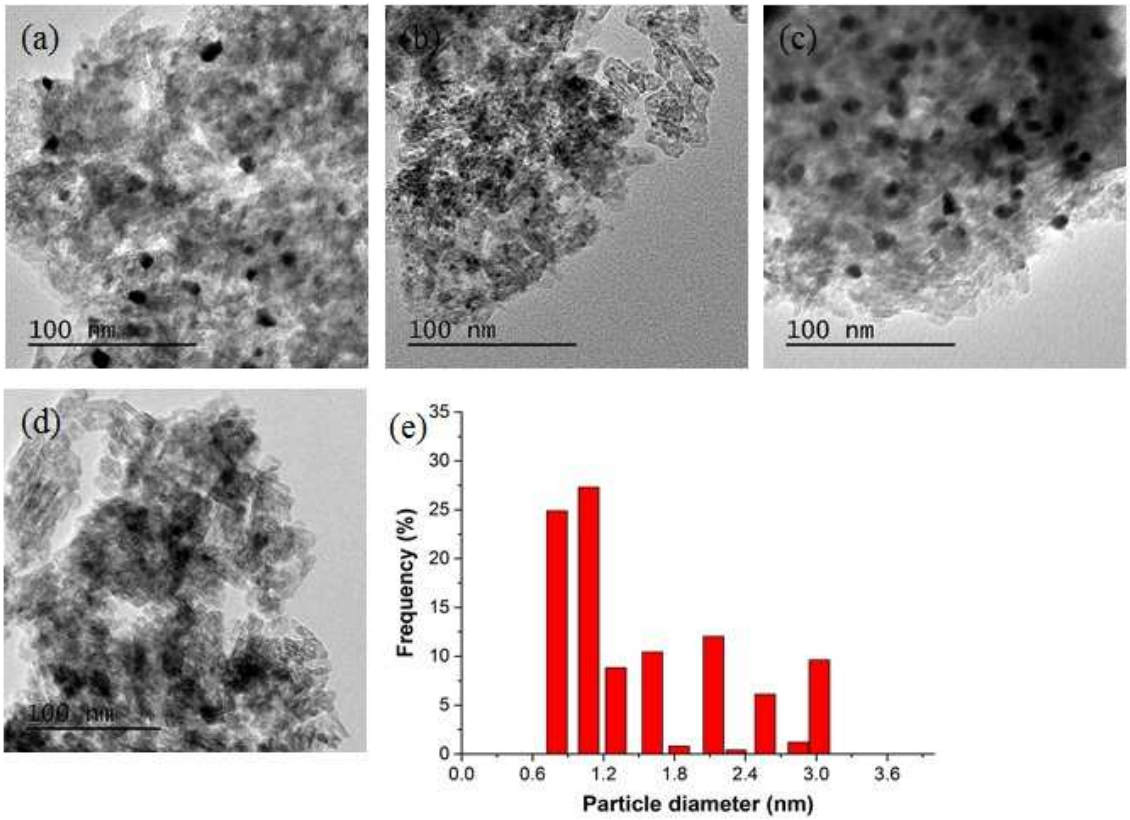
(a)
100 nm
(b)
100 nm
(c)
100 nm
(d)
100 nm
(e)
Frequency (%)
0
5
10
15
20
25
30
35
0.0
0.6
1.2
1.8
2.4
3.0
3.6
Particle diameter (nm)

Fig. 3

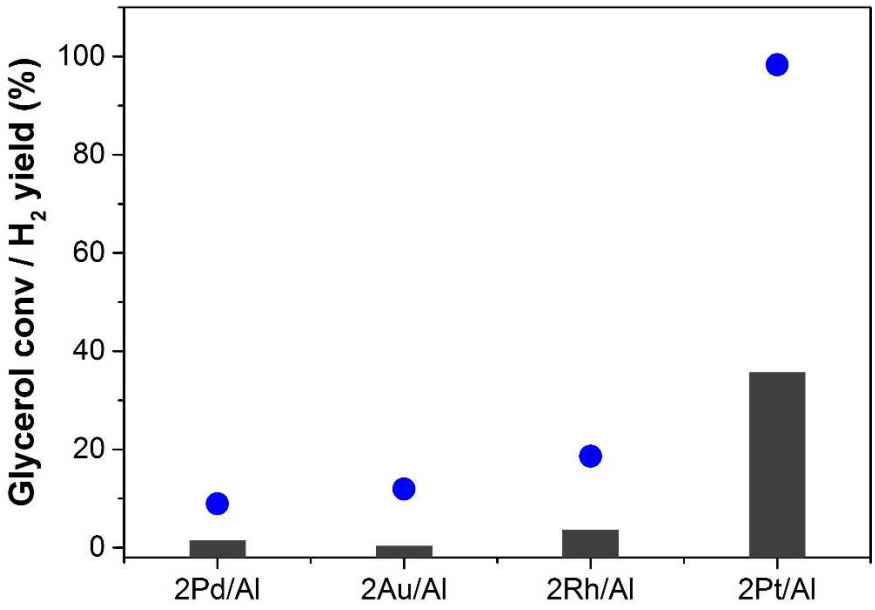
Glycerol conv / H_2 yield (%)
100
80
60
40
20
0
2Pd/Al
2Au/Al
2Rh/Al
2Pt/Al

Fig. 4

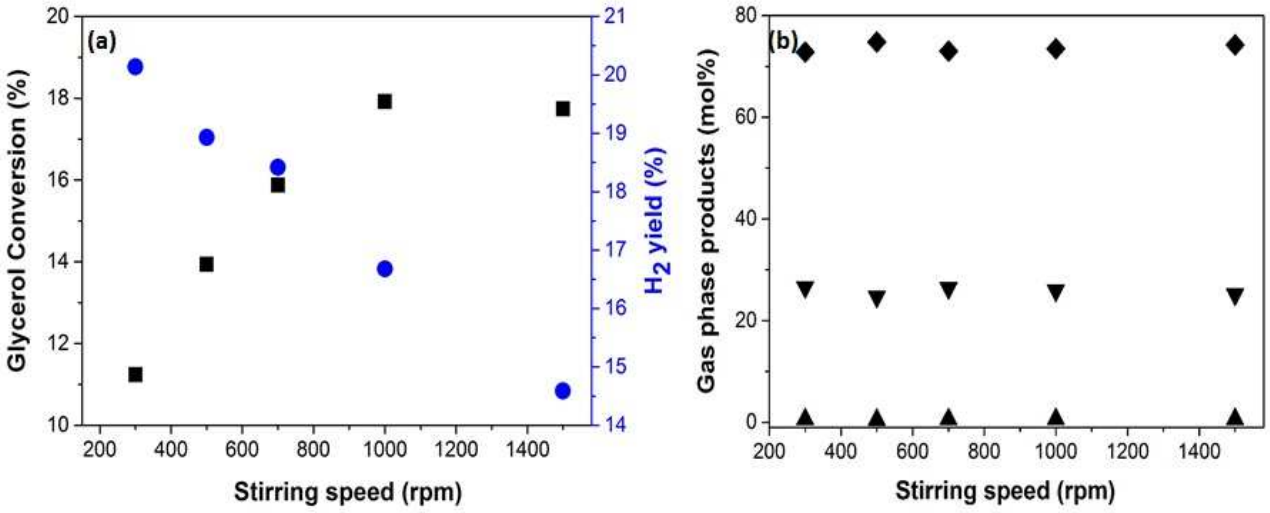
(a)
Glycerol Conversion (%)
H_2 yield (%)
Stirring speed (rpm)
(b)
Gas phase products (mol%)
Stirring speed (rpm)

Fig. 5

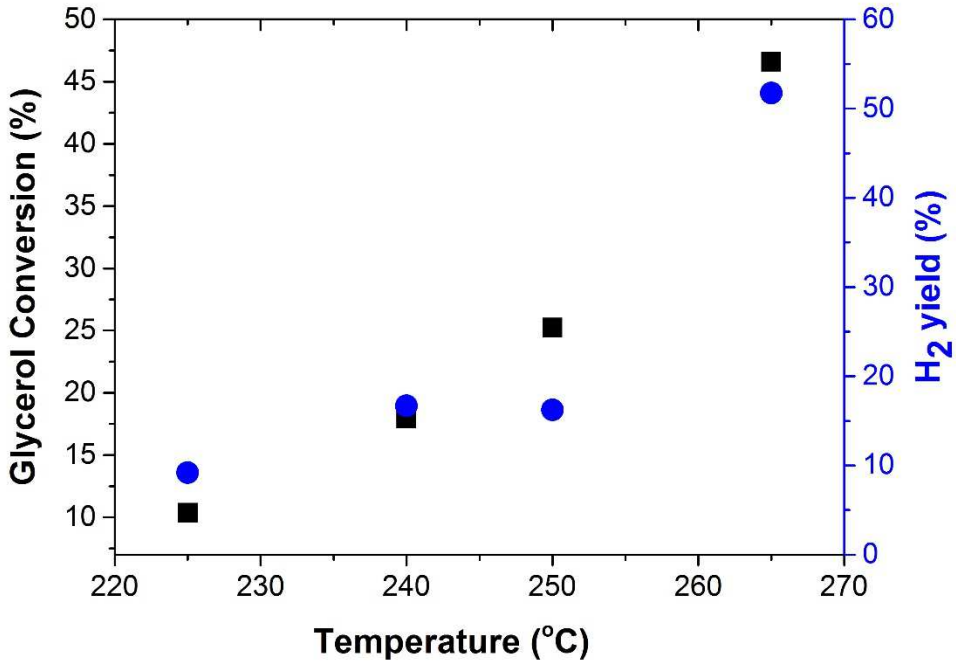
Glycerol Conversion (%)
H_2 yield (%)
Temperature (°C)
50
45
40
35
30
25
20
15
10
60
50
40
30
20
10
0
220
230
240
250
260
270

Fig. 6

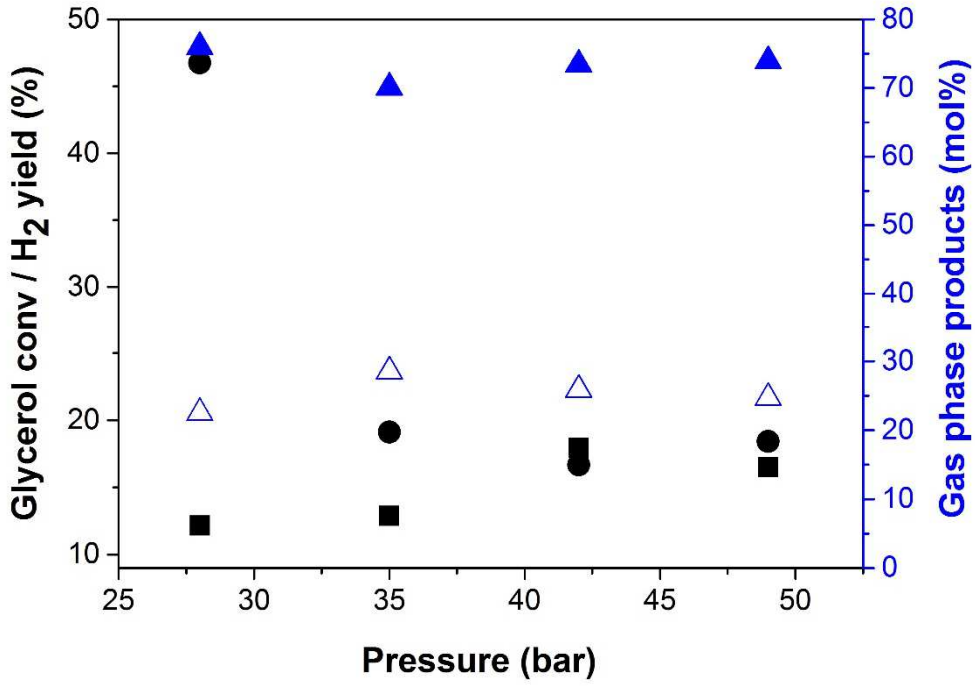
Glycerol conv / H_2 yield (%)
Gas phase products (mol%)
Pressure (bar)
50
40
30
20
10
80
70
60
50
40
30
20
10
0
25
30
35
40
45
50

Fig. 7

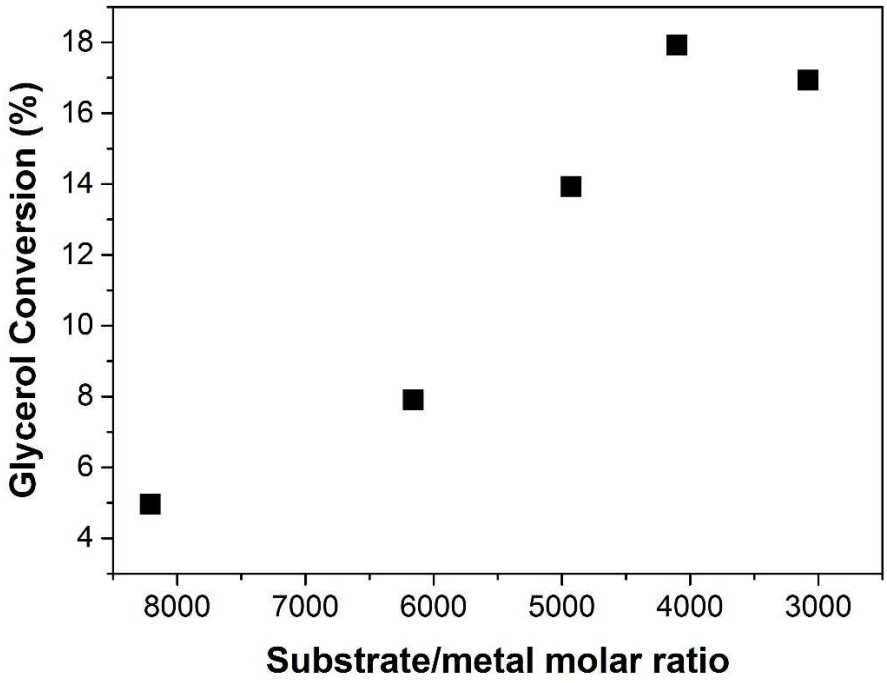
Glycerol Conversion (%)
Substrate/metal molar ratio
18
16
14
12
10
8
6
4
8000
7000
6000
5000
4000
3000

Fig. 8

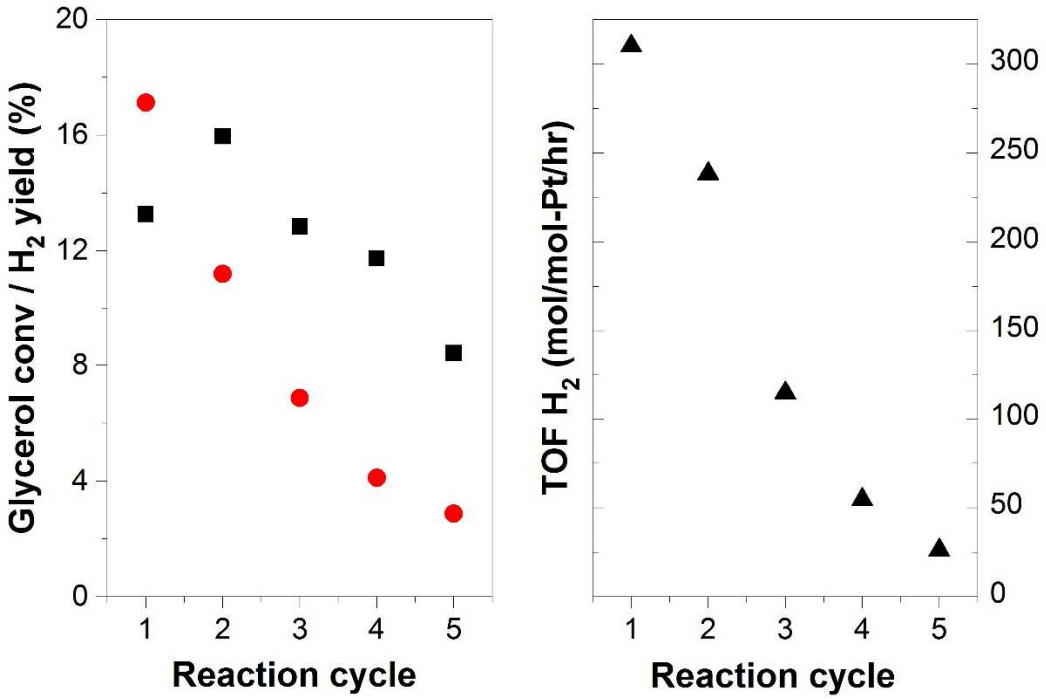
Glycerol conv / H_2 yield (%)
Reaction cycle
TOF H_2 (mol/mol-Pt/hr)
Reaction cycle

Fig. 9

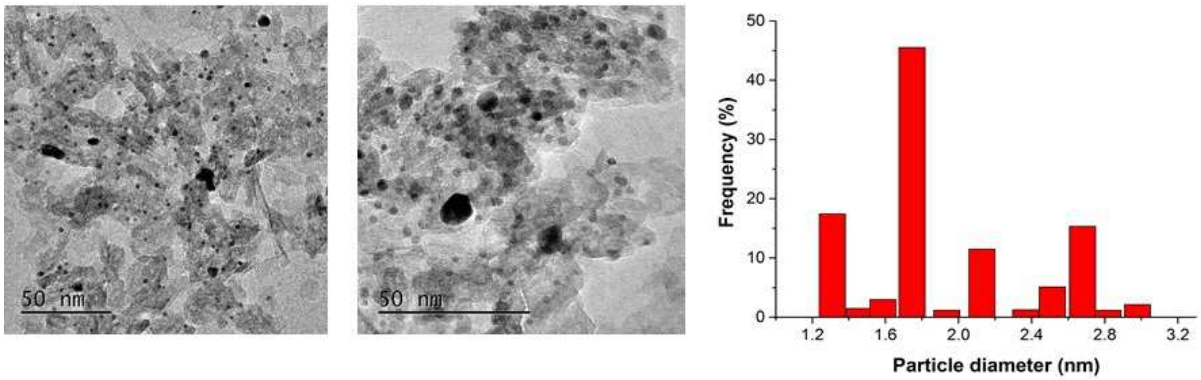
50 nm
50 nm
Frequency (%)
Particle diameter (nm)

Fig. 10

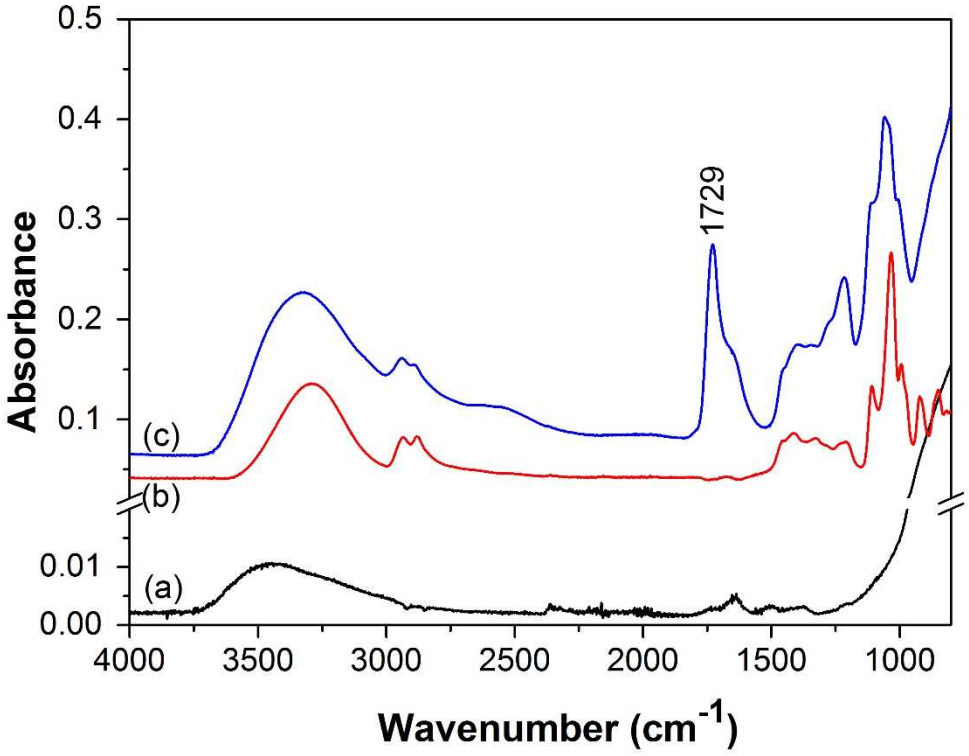
0.5
0.4
0.3
0.2
0.1
0.01
0.00
Absorbance
1729
(c)
(b)
(a)
4000
3500
3000
2500
2000
1500
1000
Wavenumber (cm-1)